International Forum on Aeroelasticity and Structural Dynamics
IFASD 2024
17-21 June 2024, The Hague, The Netherlands

APPLICATION OF SHAPE MEMORY ALLOYS FOR FLUTTER SUPPRESSION IN A PROPELLER-DRIVEN TYPICAL SECTION

Ximenes, Í.B.O[1], Silva, R.G.A.[1], Silva, F.M[1], Donadon, M.V.[1]

[1]Aeronautical Technology Institute (ITA)
Praça Marechal Eduardo Gomes, 50, 12228-900, São José Dos Campos, Brazil
italoibox@fab.mil.br
gil@ita.br
f.miranda_ppgm@poli.ufrj.br
prof.donadon@gmail.com

Keywords: Whirl Flutter (WF), Shape Memory Alloy (SMA), Typical Section (TS)

Abstract: Future aerial mobility will likely be powered by propeller propulsion, as it is more suitable for use in combination with electric motors. Therefore avoiding rotor instabilities becomes a major concern in the early project phases for the next generation of aircraft. Within this context, this work focuses on the application of Shape Memory Alloys (SMA) for Whirl Flutter (WF) suppression in propeller-driven aircraft. SMAs have a thermal-dependent modulus of elasticity, which allows the use of this class of materials to locally control the stiffness of the connections between the motor and the wing. For most of the flight, the mounting stiffness could be maintained at a minimum to better isolate the vibration coming from the motor, and only at high speeds it could be increased to avoid aeroelastic instabilities. To conduct the study, a 4 degree of freedom (dof) model of a wing section with an installed rotor was implemented and verified. This model combines a typical aeroelastic section, with springs associated with pitch and plunge dof, and the classical rotor model used in WF studies, which idealizes the rotor mounting by two torsion springs associated with pitch and yaw dof. Predictions obtained using the proposed model were compared with previous results from the literature. Following the model verification, the application of SMA was implemented by assuming that the connecting stiffness associated with the rotor installation is dependent on temperature, simulating an SMA-made mounting. Thus, it was possible to map the final flutter velocity of the system as a function of the temperatures associated with the rotor installation. The obtained results demonstrate that the flutter speed of the system may be significantly modified using this approach. They also indicate that the control of the SMA temperature shifts the dominant flutter mechanism from WF to the classical wing flutter, increasing even more the flutter speed of the system.

1 INTRODUCTION

New aircraft concepts are bringing back the use of propeller-based propulsion aiming a reduction in the environmental impact of the aviation. Once the propellers provides major efficiency in low speeds and they can be used with electric motors. Moreover, the use of electric motors enables greater flexibility in the positioning of the propellers encouraging its installation spread over all the aircraft plant. Thereby these new tendencies are influencing the next aircraft to have more propellers, installed on unusual positions and with new combinations. In this context, the Whirl Flutter analysis can became one of the most important studies in their projects.

Whirl Flutter (WF), or gyroscopic flutter, is an aeroelastic instability driven by: the gyroscopic effect due to propeller rotation, the propeller aerodynamic side forces and the intrinsic elastic

forces of the propeller mounting [1]. WF occurs when the wobbling motion of the propeller mounting turns unstable at certain flight velocity.

WF was wholly modeled by Reed III and Bland [1] for the first time in 1961. They used the structural and gyroscopic model of Taylor and Browne [2] combined with the aerodynamic model of Ribner [3, 4]for propeller side forces to obtain the velocity where the whirl mode becomes unstable. Thereafter, in 1962, Houbolt and Reed III [5] refined the model by creating a new approach for the aerodynamic side forces evaluation.

In 1964, Bennett and Bland [6] conducted very important work that, for the first time, created a model for investigating aeroelastic instabilities in a system composed of a wing with an installed rotor. They developed an analytical model combining the traditional aeroelastic models for wing flutter and WF. They concluded that the combined model was more suitable for determining which mechanism would lead the system to instability and consequently generated more precise values for the system's critical velocity.

Besides all these studies, only after two fatal accidents [7] in 1959 and 1960 the phenomena become a cause of major concern for the project of turboprop aircraft. Traditionally the approach to deal with this type of instability during the project is only avoid the critical flutter velocity, i.e., restrict the aircraft's flight envelope. However new approaches probably will became necessary to avoid whirl flutter for the forthcoming generation of turboprop aircraft. Thereby it is justified to study the feasibility of using smart materials for this propose, especially Shape Memory Alloys (SMA).

SMAs have a thermal-dependent modulus of elasticity, which allows the use of this class of materials to locally control the stiffness of the connections between the motor and the wing. For most of the flight, the mounting stiffness could be maintained at a minimum to better isolate the vibration coming from the motor, and only at high speeds, it could be increased to avoid aeroelastic instabilities. The use of SMAs for this purpose has been studied for both wing [8, 9] and panel [10, 11] flutter. This work proposes to extend the applicability of this method to control WF as well.

2 AEROELASTIC MODEL FORMULATION

To conduct the study, a four degree of freedom model of a Typical Wing Section (TS) with a installed rotor was implemented. This model combines the classical TS model presented in several textbooks of aeroelasticity, with the most common WF model described in [1] and [5]. That combination generates a model with four degrees of freedom (dofs). The purpose of this combination is to analyze somehow the influence of the wing in the phenomena without increasing too much the complexity of the model. With the same purpose the influence of the blowing caused by the rotor in the TS will be neglected too.

Both the WF and the TS classical models will be presented before the final 4 dof model. Not only for conceptual contextualization but also because the 4 dof formulation will be constructed using elements from the previous models. The definitions of each variable utilized in the formulations are outlined in tables 1, 2 and 3.

2.1 Classic WF model

Taylor and Browne [2] purposed that the movement of the rotor mounted in the aircraft could be reasonably described by two orthogonal angular displacements, pitch and yaw, has illustrated

in figure 1. Thus, overall behavior of the mounting structure can be idealized by two torsional stiffness and dampers associated with these angular movements. They also considered that the propeller had three blades or more rigid to the hub. That consideration resulted in a constant mass matrix for the system.

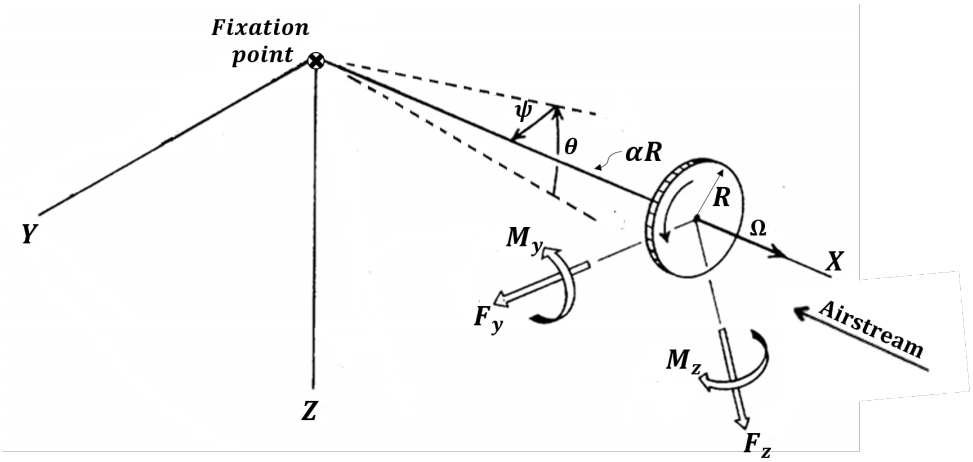

Figure 1: Reed Referential for WF Analyses (adapted from [1])

Figure 1 represents the referential adopted by [1] to his analyses as well the aerodynamic sides forces and moments acting on the structure, (F_y, F_z, M_y, M_z). Equation 14 represents the system dynamics. It can be obtained simply using the Newton's Second Law of Rotation considering a small perturbation from the equilibrium position.

$$[m_p]\ddot{q_p} + ([c_p] + [g])\dot{q_p} + [k_p]q_p = Q_p \tag{1}$$

Where

$$[m_p] = \begin{bmatrix} I_\theta & 0 \\ 0 & I_\psi \end{bmatrix}; [c_p] = \begin{bmatrix} c_\theta & 0 \\ 0 & c_\psi \end{bmatrix}; [k_p] = \begin{bmatrix} k_\theta & 0 \\ 0 & k_\psi \end{bmatrix}; [g] = I_x\omega \begin{bmatrix} 0 & 1 \\ -1 & 0 \end{bmatrix};$$

$$Q_p = \begin{bmatrix} M_y - \alpha R F_z \\ M_z + \alpha R F_y \end{bmatrix}; q_p = \begin{bmatrix} \theta \\ \psi \end{bmatrix};$$

The left side of the equation 14 can be obtained by any theory that describes lateral forces and moments actuating on the propeller. Ribner in [4] proved that lateral forces and movements depend only on pitch and yaw angles and their temporal derivatives for propeller with three or more blades. Thus, such forces and moments can be written as a function of aerodynamic constants coefficients as in equations 2,3,4 and 5.

$$F_z = \frac{1}{2}\rho V^2 \pi R \left(c_{z\theta}\overline{\theta} + c_{zq}\left(\frac{R}{V}\right)\dot{\overline{\theta}} + c_{z\psi}\overline{\psi} + c_{zq}\left(\frac{R}{V}\right)\dot{\overline{\psi}} \right) \tag{2}$$

$$F_y = \frac{1}{2}\rho V^2 \pi R \left(c_{y\theta}\overline{\theta} + c_{yq}\left(\frac{R}{V}\right)\dot{\overline{\theta}} + c_{y\psi}\overline{\psi} + c_{yq}\left(\frac{R}{V}\right)\dot{\overline{\psi}} \right) \tag{3}$$

$$M_z = \rho V^2 \pi R^2 \left(c_{m\theta}\overline{\theta} + c_{mq}\left(\frac{R}{V}\right)\dot{\overline{\theta}} + c_{m\psi}\overline{\psi} + c_{mq}\left(\frac{R}{V}\right)\dot{\overline{\psi}} \right) \tag{4}$$

$$M_y = \rho V^2 \pi R^2 \left(c_{n\theta}\overline{\theta} + c_{nq}\left(\frac{R}{V}\right)\dot{\overline{\theta}} + c_{n\psi}\overline{\psi} + c_{nq}\left(\frac{R}{V}\right)\dot{\overline{\psi}} \right) \tag{5}$$

Where $\overline{\theta}$ and $\overline{\psi}$ are the effective pitch and yaw angles of incidence of the air stream in the propeller during the whirling motion. According to [1] these effective angler are given by:

$$\overline{\theta} = \theta - \frac{\alpha R \dot{\theta}}{V} \tag{6}$$

$$\overline{\psi} = \psi + \frac{\alpha R \dot{\psi}}{V} \tag{7}$$

With some algebraic manipulations using equations 2,3,4, 5, 7 e 7 it is possible obtain a expression for Q_p:

$$Q_p = \frac{1}{2}\rho\pi R^3 (V^2[D][E][F_1]q_p + RV[D][E][F2]\dot{q_p} + R^2[D][E][F3]\ddot{q_p}); \tag{8}$$

Where

$$[D] = \begin{bmatrix} -\alpha & 0 & 1 & 0 \\ 0 & \alpha & 0 & 1 \end{bmatrix}; [E] = \begin{bmatrix} c_{z\theta} & c_{zq} & c_{z\psi} & c_{zr} \\ c_{y\theta} & c_{yq} & c_{y\psi} & c_{yr} \\ 2c_{m\theta} & 2c_{mq} & 2c_{m\psi} & 2c_{mr} \\ 2c_{n\theta} & 2c_{nq} & 2c_{n\psi} & 2c_{nr} \end{bmatrix};$$

$$[F_1] = \begin{bmatrix} 1 & 0 \\ 0 & 0 \\ 0 & 1 \\ 0 & 0 \end{bmatrix}; [F_2] = \begin{bmatrix} -\alpha & 0 \\ 1 & 0 \\ 0 & -\alpha \\ 0 & 1 \end{bmatrix}; [F_3] = \begin{bmatrix} 1 & 0 \\ 0 & 0 \\ 0 & 1 \\ 0 & 0 \end{bmatrix};$$

As previously mentioned, any consistent aerodynamic theory can be used to obtain the aerodynamic coefficients of side forces. The formulations chosen for this work are the ones developed in [5] and [12]. The first one is a quasi-steady (QS) aerodynamic formulation and second is based on the first but taking into consideration unsteady (US) aerodynamic effects. In both cases, the authors recommend suppress the terms that depends on the second derivative of the angles. Thus, the final WF model became:

$$[m_p]\ddot{q_p} + ([c_p] + [c_p^{aed}] + [g])\dot{q_p} + ([k_p] + [k_p^{aed}])q_p = 0; \tag{9}$$

The new matrices $[c_p^{aed}]$ e $[k_p^{aed}]$ are called aerodynamic stiffness and damping matrices of the system and are given by:

$$[c_p^{aed}] = -\frac{1}{2}\rho\pi R^4 V[D][E][F_2] \tag{10}$$

$$[k_p^{aed}] = -\frac{1}{2}\rho\pi R^3 V^2[D][E][F_2] \tag{11}$$

2.2 Typical Section Alone

The aeroelastic model for TF considers that the section has two possible movements[1], pitch (ϕ) and plunge (h), and that each of these degrees of freedom are associated with a stiffness and a damping. Equation 12, adapted from [13] represents it mathematically.

$$[m_w]\ddot{q_w} + [c_w]\dot{q_w} + [k_w]q_w = Q_w \tag{12}$$

Where

$$[m_w] = \begin{bmatrix} m & S_w \\ S_w & I_\phi \end{bmatrix}; [c_w] = \begin{bmatrix} c_h & 0 \\ 0 & c_\phi \end{bmatrix}; [k_r] = \begin{bmatrix} k_h & 0 \\ 0 & k_\phi \end{bmatrix};$$

$$Q_w = \begin{bmatrix} -L \\ M \end{bmatrix}; q_w = \begin{bmatrix} h \\ \phi \end{bmatrix};$$

The vector Q_w clusters the aerodynamic lift (L) and momentum (M) exerted on the typical section. The negative sign in the lift arises from the chosen reference frame for analysis, see figure 2. Following the same steps of the previous section the Q_w can be written in terms of constant aerodynamic coefficients. Several textbooks of aeroelasticity presents formulations for then. The QS and US formulations that will be used can be found in [14].

$$Q_w = \begin{bmatrix} -L \\ M \end{bmatrix} = -\rho V \begin{bmatrix} bL_{\dot{h}} & b^2 L_{\dot{\theta}} \\ -b^2 M_{\dot{h}} & -b^3 M_{\dot{\theta}} \end{bmatrix} \dot{q_w} - \rho V^2 \begin{bmatrix} L_h & bL_\theta \\ -bM_h & -b^2 M_\theta \end{bmatrix} q_w = -[c_w^{aed}]\dot{q_w} - [k_w^{aed}]q_w \tag{13}$$

Finally, the final model for the typical section alone becomes:

$$[m_w]\ddot{q_w} + ([c_w] + [c_w^{aed}])\dot{q_w} + ([k_w] + [k_w^{aed}])q_w = 0; \tag{14}$$

Similarly the new matrices $[c_w^{aed}]$ e $[k_w^{aed}]$ are also aerodynamic stiffness and damping for the TS model.

[1] see figure 2

2.3 Final 4 dof Model

Figure 2 represents the adopted referential to analyze the system consisting of the typical section with a coupled rotor. The angles θ and ψ still represent the pitch and yaw motion of the propeller with respect to the airstream. The angle ϕ represents the pitch of the section and the displacement h the plunge. This choice of variables is little different from the work done in [6]. It was done only to decouple the resultant gyroscopic matrix of system. Besides the figure 2 represents two articulations points, this works will considers a model with only one articulation point.

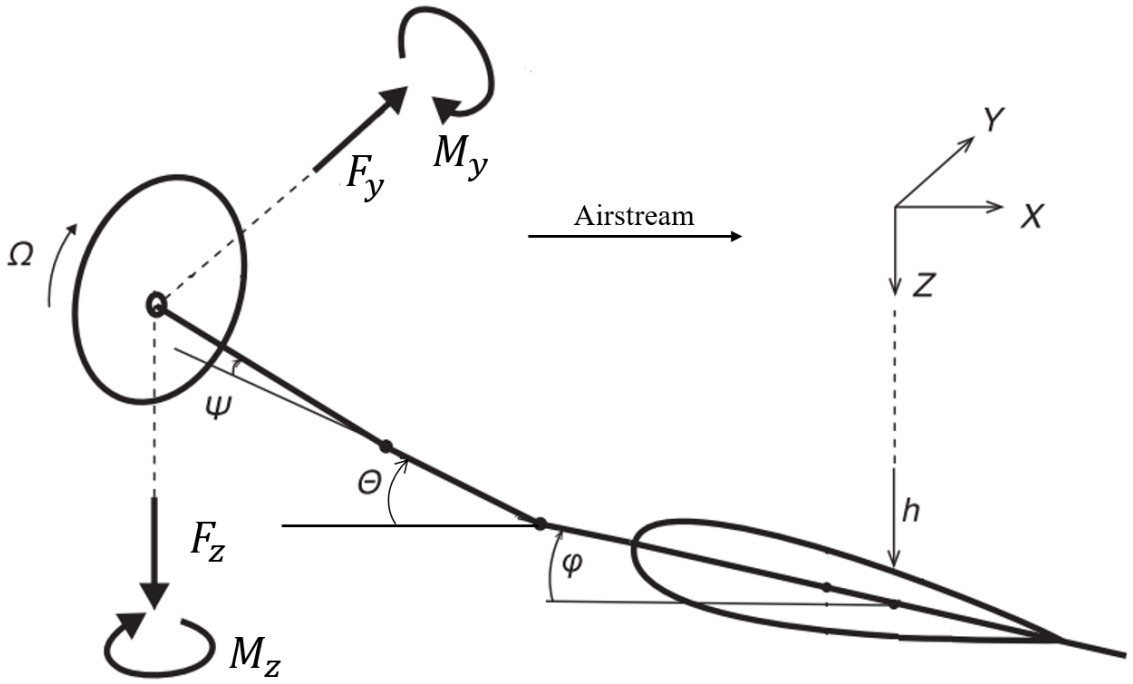

Figure 2: Propeller and TS referential (adapted from [15])

To determine the final mathematical model for the system with 4 dof the same process done in [6] can be realized, just adapting the variables names and definitions. The final model then becomes:

$$([M_p]+[M_w])\ddot{q}+([C_p]+[C_w]+[C_p^{aed}]+[C_w^{aed}]+[G])\dot{q}+([K_p]+[K_w]+[K_p^{aed}]+[K_w^{aed}])q=0; \tag{15}$$

The vector q clusters all variables in the final problem i.e.:

$$q=\begin{bmatrix}q_p\\q_w\end{bmatrix}=\begin{bmatrix}\theta\\\psi\\h\\\phi\end{bmatrix} \tag{16}$$

The matrices $[M_r]$ and $[M_w]$ represents the total inertia of the non-rotating parts of the propeller and TS respectively in terms of the new variables. They are given by:

$$[M_p] = \begin{bmatrix} & & m'x_b & m'x_b\Delta x_b \\ & [m_p] & 0 & 0 \\ m'x_b & 0 & m' & mx'_b \\ m'x_b\Delta x_b & 0 & m'x_b & m'x_b^2 \end{bmatrix} \tag{17}$$

$$[M_w] = \begin{bmatrix} 0_{2x2} & 0_{2x2} \\ 0_{2x2} & [m_w] \end{bmatrix} \tag{18}$$

Similarly, the other matrix of the final system can be determined using inherited information from the previous models.

$$[C_p] = \begin{bmatrix} & & 0 & -c_\theta \\ & [c_p] & 0 & 0 \\ 0 & 0 & 0 & 0 \\ -c_\theta & 0 & 0 & c_\theta \end{bmatrix} \tag{19}$$

$$[K_p] = \begin{bmatrix} & & 0 & -k_\theta \\ & [k_p] & 0 & 0 \\ 0 & 0 & 0 & 0 \\ -k_\theta & 0 & 0 & c_\theta \end{bmatrix} \tag{20}$$

$$[C_w] = \begin{bmatrix} 0_{2x2} & 0_{2x2} \\ 0_{2x2} & [c_w] \end{bmatrix} \tag{21}$$

$$[G] = \begin{bmatrix} [g] & 0_{2x2} \\ 0_{2x2} & 0_{2x2} \end{bmatrix} \tag{22}$$

$$[K_w] = \begin{bmatrix} 0_{2x2} & 0_{2x2} \\ 0_{2x2} & [k_w] \end{bmatrix} \tag{23}$$

$$[C_w^{aed}] = \begin{bmatrix} 0_{2x2} & 0_{2x2} \\ 0_{2x2} & [c_w^{aed}] \end{bmatrix} \tag{24}$$

$$[K_w^{aed}] = \begin{bmatrix} 0_{2x2} & 0_{2x2} \\ 0_{2x2} & [k_w^{aed}] \end{bmatrix} \tag{25}$$

For the aerodynamic matrices due to aerodynamic forces in the propeller, the transformation is not that simple. For then it is necessary to reformulate the intermediate matrices $[D]$, $[F_1]$ and $[F_2]$, which results in:

$$[C_p^{aed}] = \frac{1}{2}\rho\pi R^4 V[D^*][E][F_2^*] \tag{26}$$

$$[K_p^{aed}] = \frac{1}{2}\rho\pi R^3 V^2 [D^*][E][F_1^*] \tag{27}$$

Where:

$$D^* = \begin{bmatrix} & D & & \\ \frac{1}{R} & 0 & 0 & 0 \\ \gamma & 0 & 0 & 0 \end{bmatrix} \tag{28}$$

$$F_1^* = \begin{bmatrix} & \frac{1}{R} & -\gamma \\ F_1 & 0 & 0 \\ & 0 & 0 \\ & 0 & 0 \end{bmatrix} \tag{29}$$

$$F_2^* = \begin{bmatrix} & 0 & 0 \\ F_2 & \frac{1}{R} & -\gamma \\ & 0 & 0 \\ & 0 & 0 \end{bmatrix} \tag{30}$$

2.4 Thermal Stiffening

SMAs become stiffer during heating because partial transitions between martensite and austenite phase inside the material [8]. To insert the thermal stiffening effect in both model it is enough consider that the concentrated rigidities provided by the structure depends on the temperature by the same mathematical expression of the adopted SMA model. This assumption is equivalent to consider that the mounting structure is entirely made of SMA. Which is acceptable for a conceptual study. Therefore, the equation 31 models the thermal dependency of the system:

$$k_i(T) = \frac{k_i^M + k_i^A \cdot exp[(\frac{\chi}{A_f - A_s})(T - \frac{A_f + A_s}{2})]}{1 + exp[(\frac{\chi}{A_f - A_s})(T - \frac{A_f + A_s}{2})]}; i = [\theta, \psi] \tag{31}$$

3 NUMERICAL RESULTS AND DISCUSSION

3.1 Model Validation

Before studying the effect of thermal stiffening on the flutter speed of the system, it was necessary to validate the final 4 dof model. For this purpose, cases from the literature were selected for both TS and WF cases. The model was then validated for each case separately.

3.1.1 WF validation

This validation, consists of use the 4 dof model to reproduce the results of [16]. However that reference presents a classical WF model with only the 2 dof of the rotor. Therefore to recreate this scenario very large rigities were associated with the dof of the TS. Thus it was possible to guarantee that the principal dynamics of the system would be the rotor dynamics. Table 1 presents all data collected from [16] for this validation:

Table 1: WF Validation Study Case.

Description	Symbology	Value	Unit
Rotor Radius	R	0.152	m
Rotor Angular velocity	Ω	40	rad/s
Pivot length / rotor Radius	α	0.25	-
Rotating parts moment of inertia	I_x	0.000103	$kg \cdot m^2$
Pitch moment of inertia	I_θ	0.000178	$kg \cdot m^2$
Yaw moment of inertia	I_ψ	0.000178	$kg \cdot m^2$
Number of Blades	N_b	4	-
Blade Cord	c	0.026	m
Blade lift slope	c_l	2π	-
Structural Pitch Damping	c_θ	0.001	N m s rad^{-1}
Structural Yaw Damping	c_θ	0.001	N m s rad^{-1}
Structural Pitch Stiffness	k_θ	0.4	N m rad^{-1}
Structural Yaw Stiffness	k_ψ	0.4	N m rad^{-1}
Section pitch Stiffness	k_h	10^{10}	N m^{-1}
Section plunge Stiffness	k_ϕ	10^{10}	N m rad^{-1}

Figure 3 brings the aeroelastic diagrams obtained with that approach. The both the diagrams and the obtained flutter velocity are in agreement with the results of [16]. The horizontal lines in $V - \xi$ diagrans shows that the damping of the TS do not varied significantly with the inflow velocity confirming once more the results.

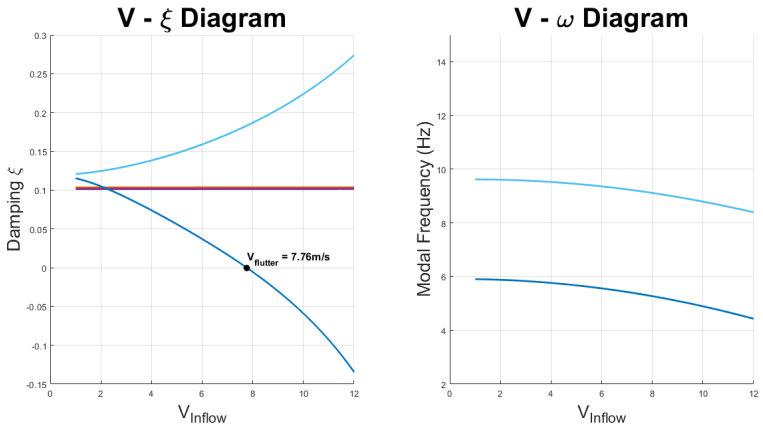

Figure 3: Aeroelastic diagrams for WF validation

The aerodynamic model used by [16] was the QS one. To also validate the US aerodynamic model a new aeroelastic diagrams were created using this formulation and compared with the previous one. The result is in figure 4. In the graphics the curves are almost indistinguishable, which allows us to conclude that use QS or US aerodynamic models for WF will results in practically the same results.

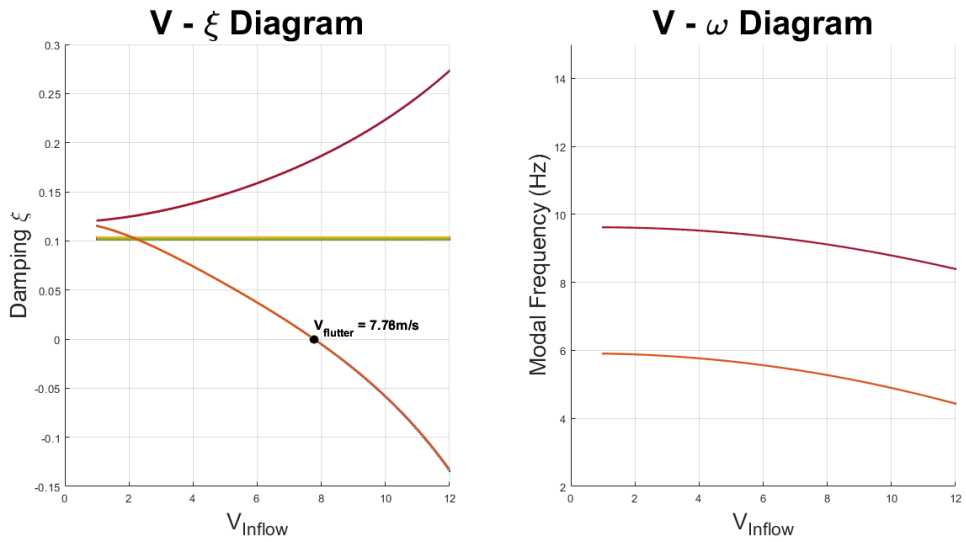

Figure 4: Comparing Aerodynamic theories

3.1.2 TS validation

Analogously to the previous section, the 4 dof model was used to reproduce results from literature. A TS study case from [13] was select for this case. The original case considers only the dofs associated with the TS so use the 4 dof model to reproduce this case it was necessary to: made the rigidities associated with the rotor much larger than the others in the study, made the mass and inertia of the rotor tend zero as well as the blade cord. Table 2 presents all data collected from [13] for this validation:

Table 2: TS Validation Study Case.

Description	Symbology	Value	Unit
Section Semi-cord	b	0.127	m
(Elastic axis location)/ b	a	-0.15	-
Section mass	m	4.7174	kg
Section Product of inertia	S_w	0.15	$kg \cdot m$
Section Moment of inertia	I_ϕ	0.0295	$kg \cdot m^2$
Section lift slope	$c_{l\alpha}$	2π	-
Structural Pitch Damping	c_ϕ	0.1	N m s rad^{-1}
Structural Plunge Damping	c_h	0.1	N m s rad^{-1}
Structural Pitch Stiffness	k_ϕ	121.2751	N rad^{-1}
Structural Plunge Stiffness	k_h	14741	N m^{-1}

The obtained diagrams and flutter speeds (figures 5 and 6) are in agreement with the ones presented in [13] for both quasi-steady and unsteady aerodynamics. It is important to perceive that the difference of aerodynamic theory is much more visible in the results for the TS.

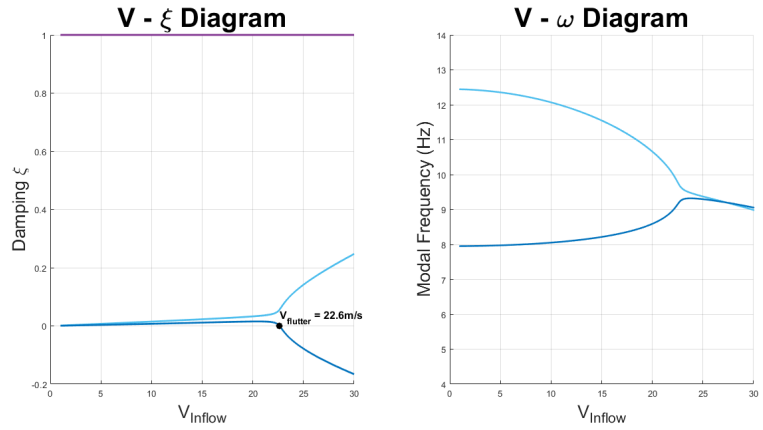

Figure 5: TS diagrams with QS Aerodynamics

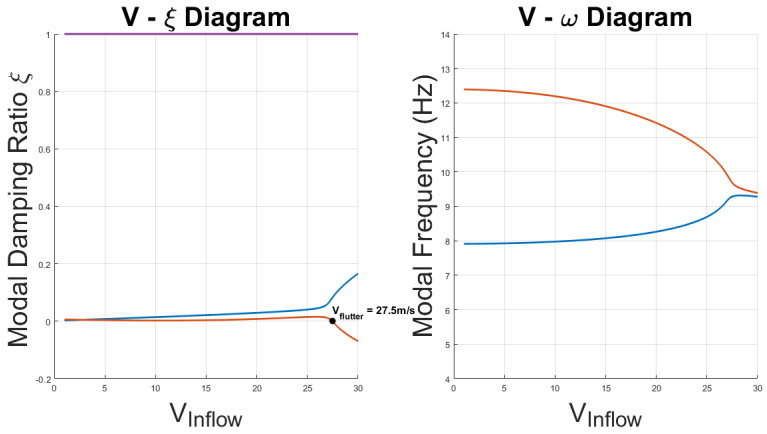

Figure 6: TS diagrams with US Aerodynamics

3.2 Thermal Stiffening Effect

With the aeroelastic model validated, the next steep is study the effect of the thermal stiffening on the flutter speed. For that, a new case of studied will be implemented combining the cases used in validation. To the combination, new variables will be introduced in the problem e.g. the X coordinate of fixation point of the rotor in the section. Some of these variables have be inferred from the previous cases and others can be chosen freely. The values adopted to that variables are presented in table 3.

Furthermore values for the variables of the thermal stiffening model have also to be determinate. To do that it was considered that the material of the connection of the rotor with the section is made of the SMA studied in [9]. Consequently the stiffness after the phase transition in the material will be three times the stiffness before as well as the spring constants used in the model for the dof associated with the propeller. The values for those variables are also in table 3.

Table 3: Thermal Stiffening Effect study.

Description	Symbology	Value	Unit
Propepller mass	m'	0.1233	kg
Propepller Fixation point	$x_b = \gamma R$	0	m
Propepller Center of Mass	x_d	-0.038	m
$x_d - x_b$	Δx_b	-0.038	m
Connection Stiffness at martensite phase	$k_{\theta,\psi}^{M_f}$	0.4	$N \cdot m^{-1}$
Connection Stiffness at austensite phase	$k_{\theta,\psi}^{A_f}$	1.2	$N \cdot m^{-1}$
Start Temperature of transition	A_s	23	ºC
Final Temperature of transition	A_f	57	ºC
Rate of transitions between phases	χ	6.2	-

After implementing the new variables it was possible to map the flutter speed of the system in function of the temperatures associated with pitch and yaw of the rotor. Such mapping was made for three different cases.

For the first case, the TS was artificially suppressed, similar to the approach taken for WF validation. In the second case, the TS was included in the dynamics, using the QS aerodynamic theory. In the third case, the TS was also present, but the aerodynamic model used was the US. In all three scenarios, the QS aerodynamic theory was chosen for the propeller side forces, as it had been previously in 3.1.1 demonstrated that using this model would not cause significant differences in the results.

The obtained results for those cases are represented in the graphics of figures 7,8,9 e 10.

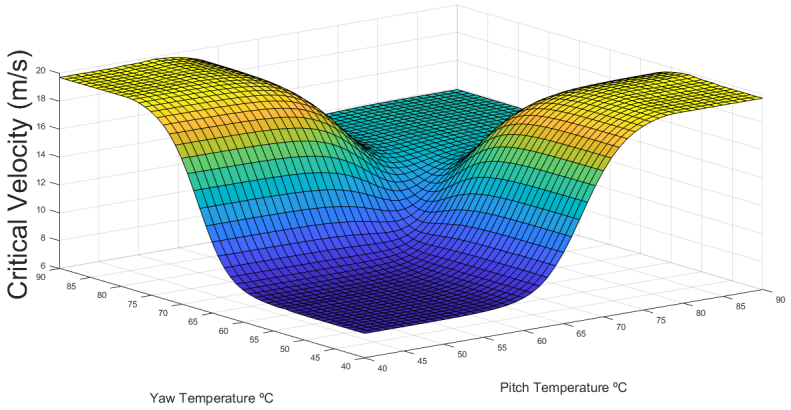

Figure 7: First Case Flutter Speed VS Temperatures

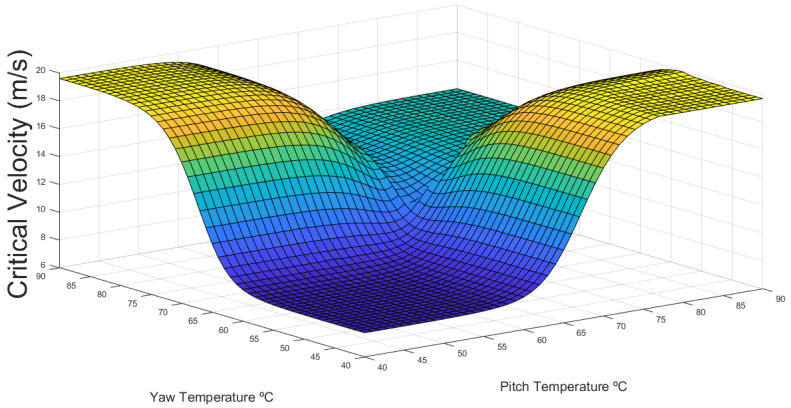

Figure 8: Second Case Flutter Speed VS Temperatures

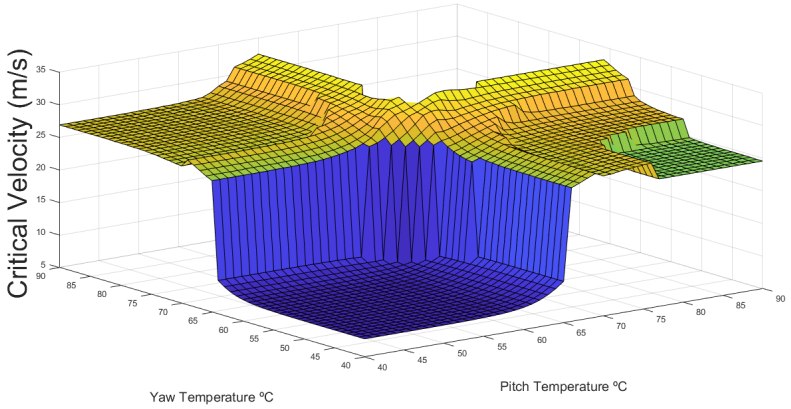

Figure 9: Thirt Case Flutter Speed VS Temperatures/ First Side

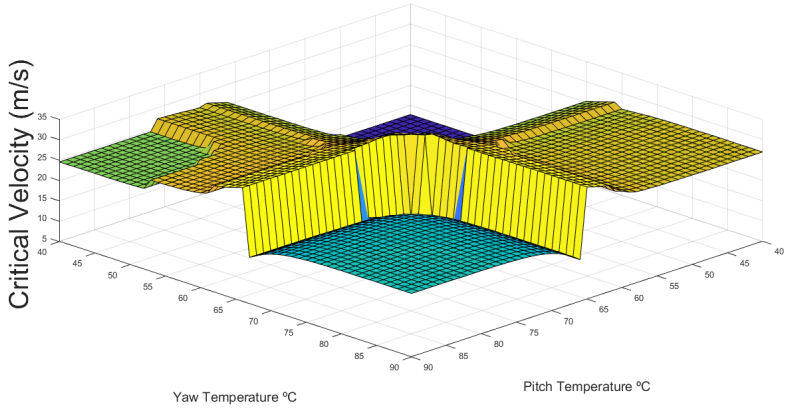

Figure 10: Thirt Case Flutter Speed VS Temperatures/ Second Side

Analysing the surfaces of figures 7,8,9 e 10 is possible to identify two important aspects. Firstly that the major flutter velocities are obtained, generally, when only one stiffness is affected by the temperature. It is in agreement with various previous results from literature [17] that established that the most susceptible configuration for WF is the symmetric one i.e. with the same rigidities associated with each propeller's dof. And secondly, that the US aerodynamic model causes great differences in the final flutter speed of the system. It was expected that the use of US

model would increase the flutter speed but it also changed the final aspect of the surface that maps the flutter speed in function of the temperatures.

To better visualise the data, graphics comparing the ”borders” of the surfaces from figures 7,8,9 e 10 were plotted in the figure 11 :

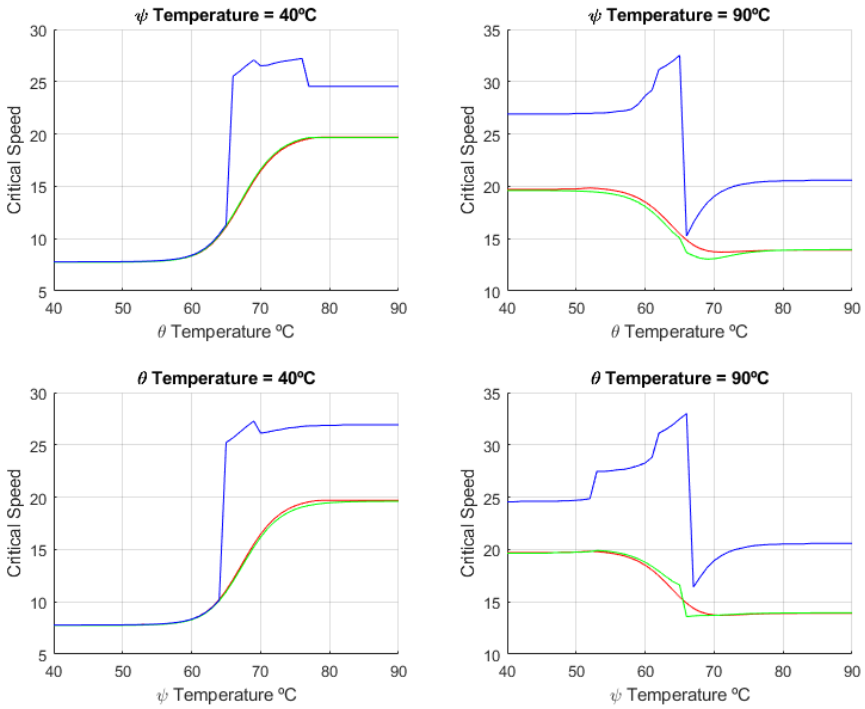

Figure 11: Results rearranged for better visualization

From the graphs in the figure 11 it is possible to infer that for low temperatures the dominant flutter mechanism is the WH for all cases studied and as the temperature increases the flutter mechanics changes depending on the case. For case 1 the flutter mechanism is WF for all temperatures since the TS dynamics has suppressed at this case. For case 2, once the flutter speed for all temperatures are very close to the obtained in case 1, it is plausible assume that the governing flutter mechanism is also WF. However for case 3 this mechanism seems to changes, between TS and WF, several times in different temperature zones, creating plateaus with small flutter speed variations separated by abrupt speed jumps. The governing flutter mechanism in each region can be determined just comparing the medium flutter speed of the region with the the flutter speeds from the validation cases.

The explanation why this happens can be found comparing the plateau of high pitch and yaw temperatures of case 3 with the behavior at the same temperature zone of the other cases. In case 3 the critical speed is about $10m/s$ bigger but the instability mechanism seems to be WF like in the other cases. The flutter speed is higher because the TS with US aerodynamics causes considerably more asymmetry for the system than the TS with QS aerodynamics and as discussed before, asymmetry of tends to stabilize the WF mechanism. This observation by the way explains why for case 3, the flutter speed is in general superior than in the other cases.

4 CONCLUSIONS

Thorough the application of canonical models of WF , TS and Thermal Stiffening of SMA it was demonstrated that is possible to significant elevate the flutter speed using some SMA based mechanism. Concluding that it is quite practicable mechanism for augment aeroelastic stability of wings with propellers installed.

It was assumed based on literature that the equivalent stiffness of the joint between the wing and the propeller can be increased by 200% if it made of some SMA. That change elevated the flutter speed to by up to 400%. This change was only achievable if the joint is not symmetric and it is possible to variate only the stiffness associated with one direction of movement, preferably the yaw direction.

To achieve such great variation, it was necessary to model not only the dynamics of the rotor, but the combined dynamics of the rotor with the typical wing section. If the section is suppressed from the model the gain in flutter speed is not more than 150%. Apparently the inclusion of the TS in the model brings more asymmetry for the system, increasing it's total stability. The gains of flutter speed also seems to be strongly dependant of the aerodynamic model used in the wing section. Using a QS model implied in the same gains calculated for the system without the TS dynamics included.

For future works more realistic study case could be analysed by the same methodology. In this case the dynamics of the complete wing could be take in consideration. And realistic values for the variables could be used. The mounting could also not be totally made of some SMA but instead SMA could be infused in the connection structure. Which would lead to minor variations in the mounting stiffness and consequently minor gains in flutter speed.

5 ACKNOWLEDGEMENTS

The authors wish to express their gratitude to the Sao Paulo Research Foundation, FAPESP, which has supported the present research under the Research Grants No. 21/11258-5, ENGINEERING RESEARCH CENTER FOR THE AERIAL MOBILITY OF THE FUTURE-FLYMOV. The authors also gratefully acknowledge the support for the present research provided by Conselho Nacional de Desenvolvimento, CNPq, under the Research Grant No. 309985/2013-7.

6 REFERENCES

[1] Reed, W. and Bland, S. (1961). An analytical treatment of aircraft propeller precession instability. Tech. Rep. TN D-659, NASA.

[2] Taylor, E. S. and Browne, K. A. (1938). Vibration isolation of aircraft power plants. *Journal of the Aeronautical Sciences*, 6(2), 43–49.

[3] Ribner, H. (1943). Formulas for propellers in yaw and charts of the side - force derivatives. Tech. Rep. TR-819, NACA.

[4] Ribner, H. (1943). Propellers in yaw. Tech. Rep. TR-820, NACA.

[5] Houbolt, J. and Reed (1962). Propeller – nacelle whirl flutter. *Journal of Aerospace Sciences*, 29(3), 333–346.

[6] Bennett, R. M. and Bland, S. R. (1964). Experimental and analytical investigation of propeller whirl flutter of a power-plant on a flexible wing. Tech. Rep. TN D-2399, NASA.

[7] (1993). Aircraft accident / incident, summary report: Loss of control business express, inc. beechcraft 1900c n811be near block island, rhode island, december 28, 1991. Tech. Rep. 20594, National Transportation Safety Board.

[8] Mohd Jani, J., Leary, M., Subic, A., et al. (2014). A review of shape memory alloy research, applications and opportunities. *Materials Design (1980-2015)*, 56, 1078–1113.

[9] Silva, G. C., Silvestre, F. J., and Donadon, M. V. (2022). A nonlinear aerothermoelastic model for slender composite beam-like wings with embedded shape memory alloys. *Composite Structures*, 287, 115–367.

[10] Donadon, M. V. and de Faria, A. R. (2016). Aeroelastic behavior of composite laminated shells with embedded sma wires under supersonic flow. *Aerospace Science and Technology*, 52, 157–166.

[11] de Matos Junior, O. D., Donadon, M. V., and Castro, S. G. (2017). Aeroelastic behavior of stiffened composite laminated panel with embedded sma wire using the hierarchical rayleigh–ritz method. *Composite Structures*, 181, 26–45.

[12] Rose, T. and Rodden, B. (1989). Propeller.nacelle whirl flutter addition to msc/nastran.

[13] Fung, Y. (1969). *An introduction to the theory of aeroelasticity*. Mineola, New York: Dover Publications.

[14] Jan R. Wright, J. E. C. (2014). *Introduction to Aircraft Aeroelasticity and Loads*. Hoboken, New Jersey: John Wiley Sons, Ltd.

[15] Čečrdle, J. (2015). 5 - analytical methods for whirl flutter investigation. In J. Čečrdle (Ed.), *Whirl Flutter of Turboprop Aircraft Structures*. Oxford: Woodhead Publishing, pp. 81–194.

[16] Mair, R. D. . T. B., C. (2018). Nonlinear stability analysis of whirl flutter in a rotor-nacelle system. nonlinear. *An International Journal of Nonlinear Dynamics and Chaos in Engineering Systems*, 94, 2013–2032.

[17] Reed, W. H. (1966). Propeller-rotor whirl flutter: A state-of-the-art review. *Journal of Sound and Vibration*, 4(3), 526–544.

COPYRIGHT STATEMENT